Rabbit Systemic Glucose Metabolism Map by Total-Body Dynamic PET/CT Technology

Haochen Wang
Department of General Surgery, the First Affiliated Hospital of Shandong First Medical University
Xue Xie
Science and Technology Innovation Center, Shandong First Medical University & Shandong Academy of Medical Sciences
Yanhua Duan
Department of Nuclear Medicine, the First Affiliated Hospital of Shandong First Medical University
Leiying Chai
Department of Nuclear Medicine, the First Affiliated Hospital of Shandong First Medical University
Kun Li
Department of Nuclear Medicine, the First Affiliated Hospital of Shandong First Medical University
Jianfeng Qiu (jfqiu100@gmail.com)
Science and Technology Innovation Center, Shandong First Medical University & Shandong Academy of Medical Sciences
Zhaoping Chen
Department of Nuclear Medicine, the First Affiliated Hospital of Shandong First Medical University

Research Article

Keywords: glucose metabolism, PET/CT, dynamic atlas, rabbit, 18F-FDG

Posted Date: January 20th, 2022

DOI: https://doi.org/10.21203/rs.3.rs-1241829/v1

Abstract

Background: This study evaluated total-body glucose metabolism in a preclinical lab animal, the rabbit, by employing a dynamic glucose metabolic image obtained with total-body fluorine-18 fluorodeoxyglucose (^{18}F-FDG) positron emission tomography/computed tomography (PET/CT).

Methods: The dynamic total-body PET/CT system was used to obtain glucose metabolic imaging from 10 sedated body-matched rabbits. The standard uptake value (SUV) of ^{18}F-FDG was used to evaluate glucose metabolism. In addition, the correlation between glucose metabolism and age was assessed, as well as metabolic differences of the major organs between genders and between left- and right sides.

Results: We found a statistically significant distribution of glucose in several organs across the entire body. There were no significant metabolic differences between genders and between bilateral sides in the 10 rabbits. Thereafter, we assayed the major organ SUV changes by dynamic PET/CT of the major organs. The heart, kidneys, liver, and bladder took up more ^{18}F-FDG, whereas the skeletal muscle, brain, spinal cord, and lungs incorporated less ^{18}F-FDG. The phenotype of SUV uptake was highly correlated with the physiological functions. However, the low ^{18}F-FDG uptake in the brain and spinal cord was due to sedation.

Conclusions: The total-body glucose metabolic atlas depicted with ^{18}F-FDG dynamic PET/CT may be used as a reference for assessing pathological ^{18}F-FDG uptake. Furthermore, this study could be a reference for lab animal research involving deregulated glucose metabolism.

1. Introduction

Fluorine-18 fluorodeoxyglucose (^{18}F-FDG) positron emission tomography (PET) has been widely used in clinical and preclinical research as a non-invasive examination approach for exploring animal physiology, biochemistry, and pharmacology *in vivo.* PET/computed tomography (CT) provides multiple classes of information that includes the body structure and molecular and metabolic changes (1). Combined with different radioactive-labeled nuclides, PET/CT molecular imaging exhibits a wide range of functional imaging.

Glucose is the major carbon source for cellular biosynthesis and energy generation (2). The imbalance of glycolytic rates in organs is always correlated with different metabolic intensities and oxygen uptake. For example, the brain, liver, and myocardium consistently take up more glucose and contain more mitochondria in the cytoplasm due to the high levels of their metabolism (3). As a glucose analogue, ^{18}F labeled FDG plays a key role in the study of systemic multi-organ metabolism. In PET imaging, differences detected by ^{18}F-FDG may reflect responses to cellular energy consumption.

Before total-body dynamic PET/CT, the clinical usage of PET/CT was generally limited to routine static imaging and partial detector coverage, thus limiting its range of use (4). Recently, the use of total-body

PET systems has enabled whole-body investigations in lab animals for establishing lab animal metabolic profiles. In the daily clinical procedure at our center, patients need to remain stationary for 60 min after injecting ^{18}F-FDG in dynamic and convenient PET until the distribution of the radio-labeled nuclide reaches equilibrium, before performing scanning. In this study, the total-body dynamic PET/CT scanner was used to obtain the rabbit glucose metabolic atlas of the major organs across the entire body and the distribution profile of the nuclide following intravenous injection to equilibrium.

Lab animals play a vital role in preclinical research. Total-body glucose metabolism has been mentioned in several animal models such as rats, dogs, and pigs (1, 3, 5, 6). None of the studies have examined rabbit glucose metabolism by total-body dynamic PET/CT. The aim of this work was, firstly, to evaluate the physiological glucose metabolism and to determine the normal range of SUV in New Zealand white rabbit for referencing. Secondly, the work established a new scheme to assess dynamic glycolytic rates of the major organs with ^{18}F-FDG PET/CT.

2. Results

After the rabbits were sedated, we obtained a general physiological profile: body weight (BW), body length (from the vertex to the beginning of the tail), and tested blood samples from the ear marginal vein (Table 1). We tested the representative assay index that potentially reflected the impairment of liver cells and bile duct, kidney function, liver synthesis function, and homeostasis. All lab test results were in the normal range (Table 2).

Table 1. Physiological profile of the New Zealand white rabbits.

No	Sex (M/F)	Weight (kg)	Length (mm)	Blood glucose (mmol/L)
1	M	3.55	460.5	5.77
2	M	3.51	455.6	4.11
3	M	3.0	436.5	4.54
4	M	3.54	438.2	6.01
5	M	3.18	437.5	5.59
6	M	3.46	437	5.88
7	M	2.97	408	5.10
8	F	3.34	445.5	5.23
9	F	3.43	454.2	5.98
10	F	2.1	416.9	5.56

M: male; F: Female

Table 2. Results of lab test.

Rabbit No	ALT (U/L)	AST (U/L)	ALB (g/L)	Tbil. (g/dL)	B. Crea. (μmol/L)	K^+ (mmol/L)	Na^+ (mmol/L)
1	51	15.4	42.6	0.4	64.8	3.97	142
2	40.9	32.6	56	0.2	84	3.81	143
3	23.4	27	56.1	0.3	77	4.52	149
4	33.2	40	51	1.1	111	4.41	139
5	22.9	60	39.4	0.7	51	5.37	133
6	17	67.7	36	2.2	67	3.66	141
7	31	11	41	1.0	102	4.61	134
8	41.5	43	33	0.7	73	5.01	139
9	50.2	77	43	1.7	95	4.30	146
10	16.6	50.1	38.2	0.9	52	5.55	149

ALT: alanine aminotransferase; AST: aspartate aminotransferase; ALB: albumin; Tbil: total bilirubin; B. Crea.:blood creatine

To analytically describe the glucose metabolic atlas across the whole body, we measured and compared the SUVs of the major organs and sexes of the rabbits (Figure 1). In order to focus on exploring the differences within the organs, we controlled the variables of all the rabbits, including age, body weight, and species.

We selected No. 5 and No. 7 rabbits as the model shape for male rabbit image, female rabbit image, and summation image, respectively. We then assigned the normalized SUVs of the major organs to enable reconstruction of the PET/CT fusion images (Figure 2). In these images, most of the major organs, including the liver, brain, bilateral kidneys, spinal cord, and bladder, all absorbed moderate to high density of ^{18}F-FDG. However, the skeletal muscles in the lower limbs and most of the bilateral lungs showed very little ^{18}F-FDG uptake.

The normalized SUVs between male rabbits and female rabbits were compared. No significant difference in the mean SUV of each organ was detected between different genders ($P > 0.05$). Moreover, no significant difference in the mean SUV of bilateral organs was found in any of the rabbits. Due to the large volume and functional complexity, we drew 3 VOIs, i.e., the VOIs of the left lobe, the right lobe, and the middle lobe of the liver. Subsequent analysis still revealed no significant differences between all of the rabbits.

In all organs, the glucose metabolic peak was observed in the heart, kidney, and bladder(Figure 3). Notably, clustering of all the rabbits based on the peak SUV revealed how the SUV was distributed in organs across the entire body.

In this study, we used the total-body dynamic PET/CT to draw the mean SUV–time curve(Figure 4). Except for the bladder, most organs reached a peak and arrived at the plateau stage within 60 s. Accordingly, we focused on the first 60 s to monitor the changes. We depict the curve up to 3000 s due to the characteristic curve changes observed in the bladder.

We took rabbit No. 1 as the representative sample to calculate the activity–time curve to 3000 s and reconstructed the PET images from 0s to 6s, 300s, 600s, 1800s, and 3000s (Figure 5). Images with good quality showed the ^{18}F-FDG transit from the marginal ear vein to the right ventricle and to the lung and then into the systemic circulation.

3. Discussion

The dynamic total-body PET/CT offers a highly sensitive and efficientframework for studying systemic glucose metabolism.

Brain ^{18}F-FDG accumulation varies widely because of the high rate of glucose utilization by neurons in humans. In our study, the measured SUV of ^{18}F-FDG in rabbit brains was lower than sober human brain ^{18}F-FDG uptake, which has been reported in the past, but similar to the results obtained in other lab animal studies. The lower SUV value in the rabbit brain was seemingly due to the suppression of glucose metabolism by chloral hydrate (7, 8). We observed the same phenomenon in the spinal cord, where the absorption of ^{18}F-FDG was the most similar to that in the brain, with a lower uptake rate and a lower peak value than most organs. Previous studies have found that ^{18}F-FDG uptake in the spinal cord is a heterogeneous function of age, gender, and degree of functional impairment in humans. Furthermore, in pediatric populations, ^{18}F-FDG uptake of the spinal cord was correlated with body weight (9,10,11).

The liver is an essential multifunctional organ in mammals. Several previous studies have reported that BW and body mass index (BMI) are significant factors in the physiological ^{18}F-FDG uptake of the liver (12). Despite varying chiefly in both size and shape, the BW and BMI were controlled within a small range, in order to keep the consistency of this study. The results showed that transaminase and total bilirubin, indicators of impairments of liver cells and biliary tract cells, fell within the normal range. As a result, there was no significant difference in the liver uptake rate and SUV peak of the liver in each rabbit. Liver is one of the dual blood supply organs in mammals, making the uptake complex (13, 14). Meanwhile, previous studies found that the usage of furosemide could cause an increase of ^{18}F-FDG uptake in the liver (15). This is mainly because the catabolism of furosemide occurs in the liver, thereby increasing energy consumption.

The lungs seem to have the second lowest SUV when compared with other organs that we analyzed. A previous study showed that ^{18}F-FDG was slightly detectable in the normal lung, whereas in lung tumor and acute lung injury (ALI), the SUV is expected to be elevated due to the high metabolic activity of tumor cells and neutrophils present in the lung (5, 16, 17). It is conceivable that the high SUV peak of the lung during the first minutes is mainly due to the first pass of high ^{18}F-FDG concentration in the blood pool. After the first ^{18}F-FDG pass in the blood, the pulmonary uptake of^{18}F-FDG dropped quickly to the level of the spine and brain (Figure 4**)**.

The bilateral thighs took up little ^{18}F-FDG in all the rabbits examined in our study. This appears to be due to the lack of skeletal muscle movement, as well as the use of both glucose and fatty acids as energy sources in muscle tissues (18). By contrast, the myocardium showed more and earlier consumption of ^{18}F-FDG in the dynamic images. However, individual variation was significant. Variability of ^{18}F-FDG uptake in the myocardium has been reported in humans (19, 20). Importantly, cardiac movement makes assessments challenging for manually drawing VOIs.

We accurately measured the renal parenchymal SUV and avoided contamination from other parts of the renal pelvis. In the initial ^{18}F-FDG injection stage, the kidneys absorbed the ^{18}F-FDG quickly with the peak SUV and mean SUV higher than that of most organs other than the lungs and heart. After about 300 s, the ^{18}F-FDG began to accumulate in each rabbit bladder. The clearance of ^{18}F-FDG depends substantially on the glomerular filtration rate (GFR). In the remaining scanning period, the SUV gradually increased; however, the accumulation and uptake rate varied due to water deprivation prior to scanning. The hydration of each subject varied significantly. As the previous study reported, ^{18}F-FDG accumulation was significantly reduced in the bladder when preconditioned with urethral catheterization, followed by hydration or intravenous furosemide before ^{18}F-FDG-PET analysis (15, 21).

Several limitations pertinent to the studies included in this work were the effects of sedation, which suggests there may be some discrepancies in the organ when compared with that measured when not sedated. Another limitation was that despite the uniform treatment of the rabbits, there was a high variability in the uptake of ^{18}F-FDG, which may mirror the depth of anesthesia.

4. Conclusions

We have demonstrated that it is possible to generate total body glucose metabolism map by dynamic whole-body PET/CT in rabbit.There are numerous contexts in which this model could be clinically relevant. For example, these models provide a reference standard that could be used for the interpretation of preclinical studies in older patients or those with cancer and/or deregulated glucose metabolism.

5. Methods

5.1. Subjects

Seven male and three female healthy New Zealand white rabbits were used in this study. All of the rabbits were 6 months old, and the body weights ranged from 2.95 kg to 3.71 kg (Table 1). Rabbits were acclimated in the facility for 1 week before the study. Every animal was fasted for 6 h, with free access to drinking water before scanning.

5.2 Experimental protocol

During scanning, the rabbits were fastened in the panel and sedated with 10% chloral hydrate (3 mL/kg), which was slowly injected into the ear vein. The tracer ^{18}F-FDG was then injected into the same peripheral vein in the scanning bed.

5.3 PET/CT scanning

PET/CT scanning was performed using the uEXPLORER (United Imaging Healthcare, Shanghai, China) after an intravenous injection of ^{18}F-FDG. After injection, the dynamic total-body PET/CT scan was performed with the uEXPLORER for 3600 s. All rabbits were placed in the prone position on the scanning bed.

The PET images were reconstructed using all 3600 s data, time of flight and point spread function modeling, two iterations and 20 subsets, matrix = 192 × 192, slice thickness = 2.89 mm, and pixel size = 3.125 × 3.125 × 2.886 mm^3 with a Gaussian filter (FWHM = 3 mm). All necessary corrections including attenuation and scatter correction were performed.

5.4 The measurement of ^{18}F-FDG

The volume of interest (VOI) of major organs, including those of the brain, heart, bilateral lungs, liver, bilateral kidneys, bladder, vertebra, and bilateral thighs, was drawn manually on the selected image plane, with the most intense ^{18}F-FDG uptake in each organ site identified by one radiologist and one experienced technician. At the same time, the VOIs were drawn for two or three separate parts of one organ. Thereafter, the mean SUV was automatically determined from the area selected. Mean SUVs of ^{18}F-FDG in these organs were calculated from the concentration of the radiotracer normalized according to the injected dose and body weight. The ^{18}F-FDG decay was corrected automatically by the software.

5.5 Statistical methods

Data were presented as the mean ± standard deviation. Statistical analysis was performed using GraphPad Prism 8 (GraphPad Software Inc., La Jolla, CA).

Declarations

Acknowledgment:

Funding：This work was supported by the Jinan Science and Technology Foundation [Grant No. 2020GXRC018], the Academic Promotion Program of Shandong First Medical University [Grant No. 2019QL009] and [Grant No. 2019LJ005], and the Taishan Scholars Program of Shandong Province [Grant No. TS201712065].

There is no conflict of interest related to this article.

Ethical Statement:

The study was approved by institutional ethics committee of Shandong First Medical University & Shandong Academy of Medical Science (W2021092703090), in compliance with China national guidelines for the care and use of experimental animals.

This study is reported in accordance with **ARRIVE guidelines.**

References

[1] Fletcher JW, Djulbegovic B, Soares HP, et al. Recommendations on the use of 18F-FDG PET in oncology. J Nucl Med. 2008. 49(3): 480-508.

[2] Baraille F, Planchais J, Dentin R, Guilmeau S, Postic C. Integration of ChREBP-Mediated Glucose Sensing into Whole Body Metabolism. Physiology (Bethesda). 2015. 30(6): 428-37.

[3] Jang C, Hui S, Zeng X, et al. Metabolite Exchange between Mammalian Organs Quantified in Pigs. Cell Metab. 2019. 30(3): 594-606.e3.

[4] Cherry SR, Badawi RD, Karp JS, Moses WW, Price P, Jones T. Total-body imaging: Transforming the role of positron emission tomography. Sci Transl Med. 2017. 9(381).

[5] Lee MS, Lee AR, Jung MA, et al. Characterization of physiologic 18F-FDG uptake with PET-CT in dogs. Vet Radiol Ultrasound. 2010. 51(6): 670-3.

[6] Min W, Fang P, Huang G, Shi M, Zhang Z. The decline of whole-body glucose metabolism in ovariectomized rats. Exp Gerontol. 2018. 113: 106-112.

[7] Alstrup AK, Smith DF. Anaesthesia for positron emission tomography scanning of animal brains. Lab Anim. 2013. 47(1): 12-8.

[8] Shammas A, Lim R, Charron M. Pediatric FDG PET/CT: physiologic uptake, normal variants, and benign conditions. Radiographics. 2009. 29(5): 1467-86.

[9] Amin A, Rosenbaum SJ, Bockisch A. Physiological ¹⁸F-FDG uptake by the spinal cord: is it a point of consideration for cancer patients. J Neurooncol. 2012. 107(3): 609-15.

[10] Taralli S, Leccisotti L, Mattoli MV, et al. Physiological Activity of Spinal Cord in Children: An 18F-FDG PET-CT Study. Spine (Phila Pa 1976). 2015. 40(11): E647-52.

[11] Aiello M, Alfano V, Salvatore E, et al. [(18)F]FDG uptake of the normal spinal cord in PET/MR imaging: comparison with PET/CT imaging. EJNMMI Res. 2020. 10(1): 91.

[12] Keiding S, Sørensen M, Frisch K, Gormsen LC, Munk OL. Quantitative PET of liver functions. Am J Nucl Med Mol Imaging. 2018. 8(2): 73-85.

[13] Keiding S. Bringing physiology into PET of the liver. J Nucl Med. 2012. 53(3): 425-33.

[14] Brix G, Ziegler SI, Bellemann ME, et al. Quantification of [(18)F]FDG uptake in the normal liver using dynamic PET: impact and modeling of the dual hepatic blood supply. J Nucl Med. 2001. 42(8): 1265-73.

[15] Cussó L, Desco M. Suppression of 18F-FDG signal in the bladder on small animal PET-CT. PLoS One. 2018. 13(10): e0205610.

[16] Capitanio S, Nordin AJ, Noraini AR, Rossetti C. PET/CT in nononcological lung diseases: current applications and future perspectives. Eur Respir Rev. 2016. 25(141): 247-58.

[17] Vansteenkiste JF, Stroobants SG, Dupont PJ, et al. Prognostic importance of the standardized uptake value on (18)F-fluoro-2-deoxy-glucose-positron emission tomography scan in non-small-cell lung cancer: An analysis of 125 cases. Leuven Lung Cancer Group. J Clin Oncol. 1999. 17(10): 3201-6.

[18] Engel H, Steinert H, Buck A, Berthold T, Huch Böni RA, von Schulthess GK. Whole-body PET: physiological and artifactual fluorodeoxyglucose accumulations. J Nucl Med. 1996. 37(3): 441-6.

[19] Ramos CD, Erdi YE, Gonen M, et al. FDG-PET standardized uptake values in normal anatomical structures using iterative reconstruction segmented attenuation correction and filtered back-projection. Eur J Nucl Med. 2001. 28(2): 155-64.

[20] Tan LT, Ong KL. Semi-quantitative measurements of normal organs with variable metabolic activity on FDG PET imaging. Ann Acad Med Singap. 2004. 33(2): 183-5.

[21] Kosuda S, Fisher S, Wahl RL. Animal studies on the reduction and/or dilution of 2-deoxy-2-[18F]fluoro-D-glucose (FDG) activity in the urinary system. Ann Nucl Med. 1997. 11(3): 213-8.

Figures

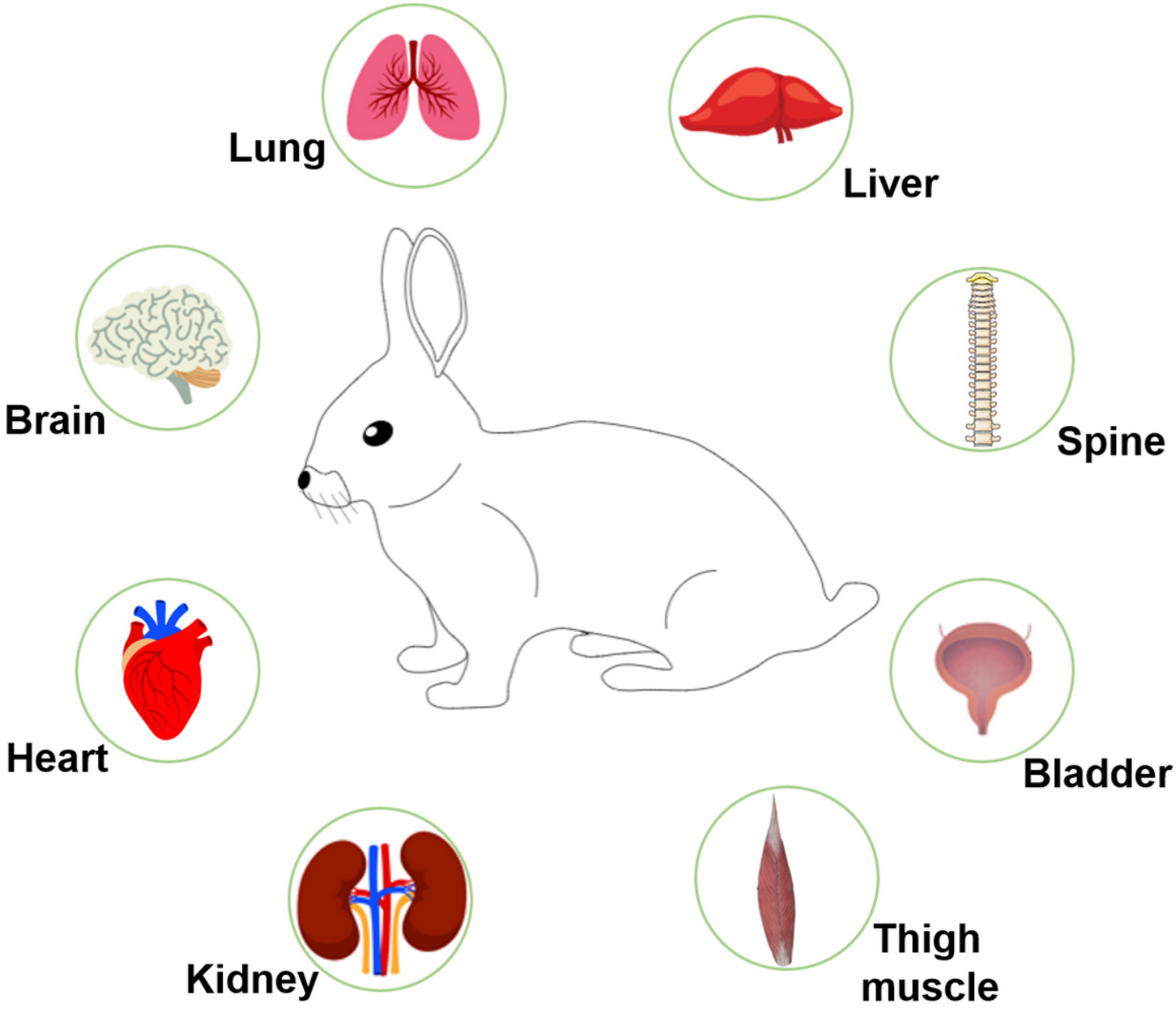

Figure 1

Schematic diagram shows the major organs analyzed for glucose metabolism activity in our study.

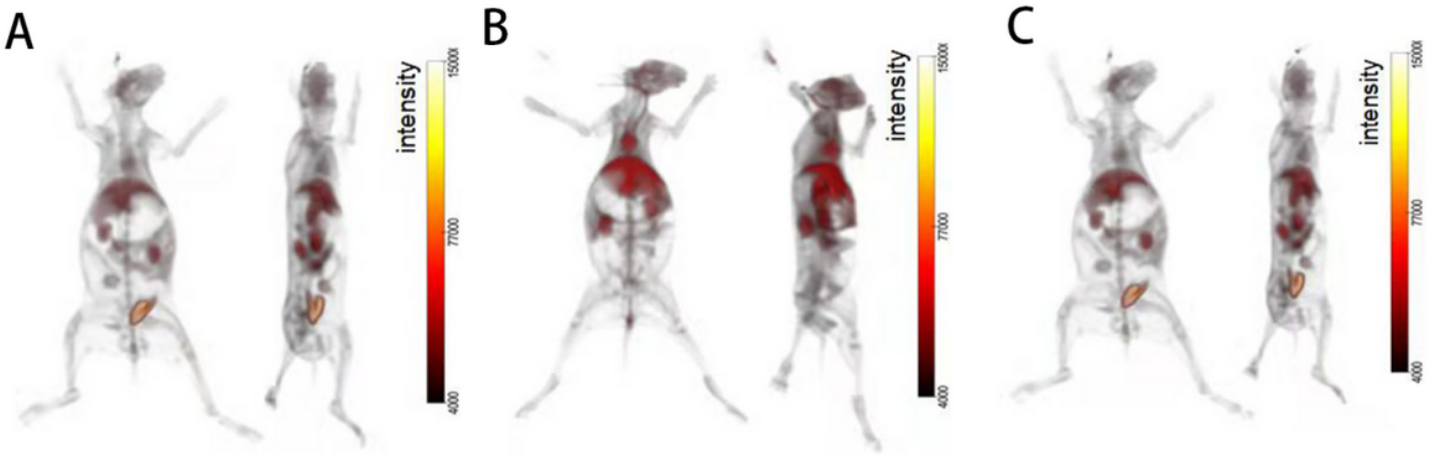

Figure 2

The SUV assignments of the major organs were those of the brain, heart, bilateral lungs, liver, bilateral kidneys, bladder, spinal cord, and bilateral thighs. Additional organs were not assigned. **(a)** The mean SUV assignment of seven male rabbits, with the No. 5 rabbit as the model shape. **(b)** The mean SUV assignment of three female rabbits, with the No. 7 rabbit as the model shape. **(c)** The mean SUV assignment of all 10 rabbits, with the No. 5 rabbit as the model shape.

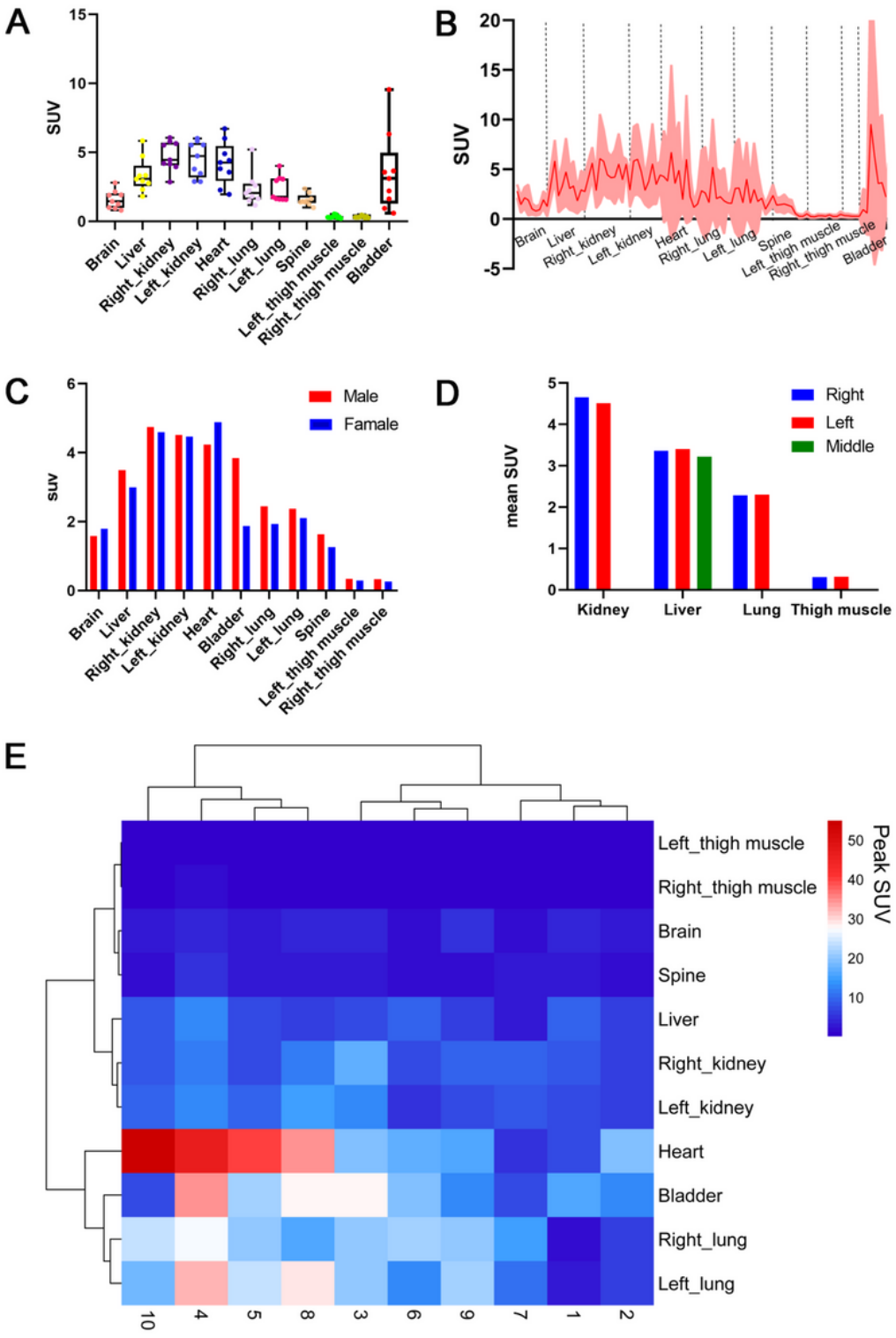

Figure 3

Glucose metabolic activities of major organs in all 10 rabbits. **(a)** Histogram of the mean SUV showing the distribution in all 10 rabbits. **(b)** Major organ comparison. The full line indicates the mean SUV of the 10 rabbits. The filled area indicates the standard deviation. **(c)** Comparisons of the glucose metabolic profiles among the different gender. **(d)** Comparisons of the glucose metabolic profiles between the different side. **(e)** Heat map of the peak SUV of the major organs across the whole body of all rabbits.

Each column represents a single rabbit, and each row represents the peak SUV of an organ. Samples were clustered using hierarchical clustering.

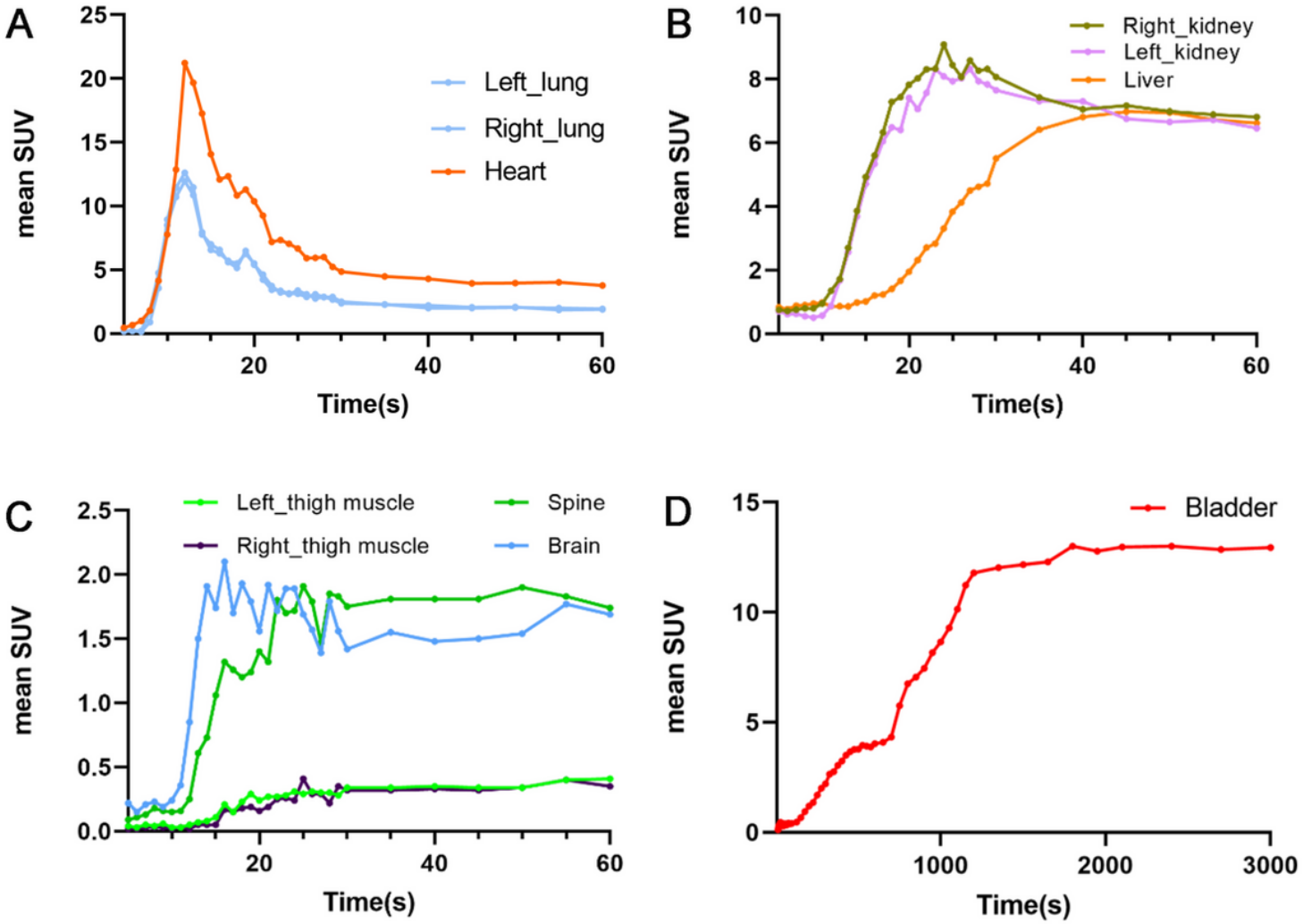

Figure 4

The mean SUV–time dynamic curves of the major organs in the 10 rabbits.

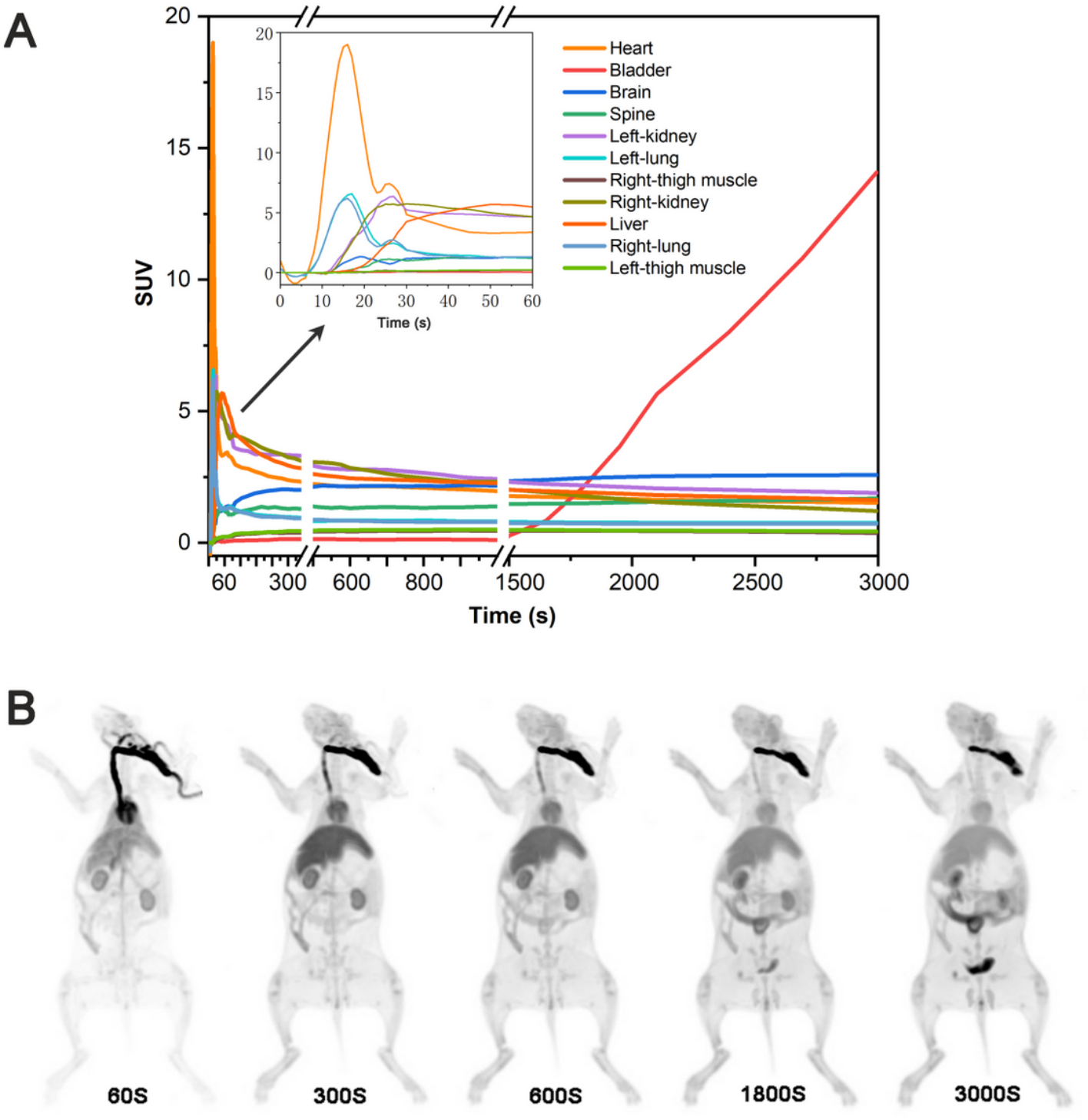

Figure 5

(a) Activity–time curve of rabbit 1. The **(a)** inset: activity–time curve for the first minute of the acquisition. **(b)** Five total-body dynamic PET/CT images in 60 second, 300 second, 600 second, 1800 second, 3000 second to show the dynamic ^{18}F-FDG distribution of rabbits. Each dynamic image is clear and shows the dynamic visual glucose uptake changes of the total-body for different anatomical regions.